

Supporting Information for

**Assessing the impact of Corona-virus-19 on nitrogen
dioxide levels over southern Ontario, Canada**

Debora Griffin¹, Chris A. McLinden^{1,2}, Jacinthe Racine³, Michael D. Moran¹, Vitali Fioletov¹,
Rabab Mashayekhi³, Radenko Pavlovic³, Xiaoyi Zhao⁴, Henk Eskes⁴

¹Air Quality Research Division, Environment and Climate Change Canada, Toronto, Ontario, Canada

²Institute of Space and Atmospheric Studies, University of Saskatchewan, Saskatoon, Canada

³Canadian Meteorological Centre Operations Division, Environment and Climate Change Canada, Dorval, Quebec,
Canada

⁴Royal Netherlands Meteorological Institute (KNMI), De Bilt, The Netherlands

Contents of this file

Text S1
Figures S1 to S10
Tables S1 to S3

Introduction

Supplementary material for "Assessing the impact of Corona-virus-19 on nitrogen dioxide levels over Southern Ontario, Canada" by D. Griffin et al. This document contains further details about the methodology used in this study to determine the alternative air mass factors (AMFs). Figures that help with the interpretation of the results, but could not be included in the main manuscript (due to size limitations) are also included here.

Text S1.

Alternative Air Mass Factors

In this study, we used alternative air mass factors (AMFs) to convert the TROPOMI slant column density (SCD) to a vertical column density (VCD). The approach is similar to most other AMF determinations (e.g. Palmer et al. 2001, Martin et al., 2002), with the difference here being the input information as described below. The TROPOMI VCD is determined using the relationship $VCD = SCD/AMF$, where it is the AMF that links the SCD to VCD

$$SCD = \sum_z nd(z) \cdot AMF(z) = VCD \cdot \frac{\sum_z nd(z) \cdot AMF(z)}{\sum_z nd(z)} = VCD \cdot AMF$$

Where $nd(z)$ is the NO₂ number density vertical profile (in our analysis we used the profile from GEM-MACH model as described below) and thus the total-column AMF is defined as:

$$AMF = \frac{\sum_z nd(z) \cdot AMF(z)}{\sum_z nd(z)}$$

And where the sum is performed over altitudes between the surface and the tropopause. The quantity $AMF(z)$ is the altitude-dependent AMF and is specific to each scene. The SASKTRAN radiative transfer model (Bourassa et al., 2008; Dueck et al., 2017; Zawada et al., 2015) was used to generate a look-up table that describes how AMFs change as a function of surface reflectivity, solar zenith angle, viewing geometry, altitude of the NO₂ layer, surface pressure, and cloud height (see Table S1 and Griffin et al., 2019). O₃ is not considered as it is not important in the wavelength used for the NO₂ retrieval. Similar as in the original TROPOMI AMF estimate, aerosols are accounted for implicitly by the cloud fraction that is sensitive to aerosols (e.g. Boersma et al., 2007). Two AMFs are estimate, one for clear sky (AMF_{cs}) and for cloudy conditions (AMF_{cd}), and the final AMF is estimated by using the cloud radiance fraction cf (from original TROPOMI file):

$$AMF = cf \cdot AMF_{cd} + (1 - cf) \cdot AMF_{cs}$$

The cloud input information, as well as the viewing geometry is taken from the original TROPOMI files. The surface albedo information is taken from MODIS (see details below), which is a higher resolution compared to the OMI climatology used in the original TROPOMI files (see Table S1). Furthermore, the surface albedo changes significantly in case of snow and ice on the ground; an improved and high-resolution snow flag from Interactive Multisensor Snow and Ice Mapping System (IMS) (Helfrich et al., 2007) at 4 km resolution was used to flag pixels with snow-cover (which has been shown to better identify snow-covered scenes (McLinden et al., 2014; Cooper et al., 2018)) and assign an appropriate surface albedo accordingly.

Table S1. Parameters and their reference points in the AMF look-up table (LUT) used for the alternative AMF estimate tropospheric vertical column. The source of the information used for the interpolation of the LUT is displayed, Note, the surface albedo is used for the estimate of the clear sky AMF, and the cloud pressure is only used for the estimate of the cloudy AMF.

Parameter	Source	Number of reference points	Reference points
Solar Zenith angle (°)	Original TROPOMI file	10	0,30,50,60,65,70,73,76,78,80
Viewing angle (°)	Original TROPOMI file	7	0,30,50,60,65,70,72

Relative azimuth angle (°)	Original TROPOMI file	7	0,30,60,90,120,150,180
Surface pressure (hPa)	GEM-MACH	4	600,800,900,1000
Surface albedo	MODIS	10	0.0,0.03,0.06,0.09, 0.12, 0.2, 0.3, 0.5, 0.75, 1.0
Absorber profile	GEM-MACH	24 altitudes	250-11,750 in steps of 500 m
Cloud pressure (hPa)	Original TROPOMI file	5	200,400,600,800,900

The information on the NO₂ profile shape is taken from ECCC's operational regional air quality forecast model; the Global Environmental Multiscale - Modelling Air-quality and Chemistry (GEM-MACH). The operational version of the model (Moran et al, 2010; Pavlovic et al., 2016; Pendlebury et al, 2018) has a 10x10km² grid cell size for a North American domain and considers 41 gas-phase chemical species a 2-size bin particulate matter (PM) size distribution, and 8 PM chemical species (sulphate, nitrate, ammonium, black carbon, primary organic matter, secondary organic matter, sea-salt, and crustal material). The meteorological component of GEM-MACH is within the physics module of the Global Environmental Multiscale (GEM) weather forecast model (Coté et al., 1998; Girard et al., 2014). Further details on GEM-MACH can be found in, e.g., Makar et al. (2015a,b), Gong et al. (2015, 2018), and Akingunola et al. (2018).

The operational forecast makes use of 2013 Canadian and 2017 projected U.S. emissions information (Zhang et al., 2018; Moran and Ménard, 2019). The emissions used in the model are processed using the Sparse Matrix Operator Kernel Emissions (SMOKE; Coats et al., 1996; Houyoux et al., 2000).

Here, we use the hourly model output for the closest hour of the measurements and the closest grid-box of the 10 km resolution version of GEM-MACH. The TM5-MP model used for the standard TROPOMI product has global coverage but with coarser horizontal spatial resolution (1°x1°, or about 111 x 80 km² at 44°N) and thus will be unable to capture fine-scale spatial gradients in the NO₂ profile distribution, due to very localized enhancements. This performance can be improved by using input from regional models. To generate an improved a priori NO₂ profiles, we use the NO₂ concentrations from 0-1.5 km from the GEM-MACH model for the closest hour of the TROPOMI overpass. Between 1.5-12 km we use the concentrations from a monthly GEOS-Chem model run at the approximate time of the TROPOMI overpass on a 0.5°x0.67° resolution version v8-03-01 (<http://www.geos-chem.org>) (Bey et al., 2001; McLinden et al., 2014), as the GEM-MACH model currently does not include NO_x sources in the free troposphere, such as lightning and aircraft emissions at cruising altitude.

MODIS provides white-sky albedo (WSA) and black-sky albedo (BSA), based on 16-day averages available every 8 days, at a resolution of 0.05°x0.05° (collection 6.1 MCD43C3; Schaaf et al., 2002). From this, a monthly-mean albedo is computed considering only 100 % snow-free pixels. For surfaces with snow-cover, a climatology of the MODIS surface reflectance is used that only includes pixels with full snow-cover. To determine whether the TROPOMI pixel is snow covered, we use the daily IMS snow flag (<http://www.natice.noaa.gov/ims/>) on a 4x4 km² resolution. It has been shown that the IMS product is better suited than other snow-products in

differentiating between snow and snow-free scenes (Cooper et al., 2018), including the NISE snow flag used for the standard TROPOMI product that has a tendency of missing thin snow layers (McLinden et al., 2014). The MODIS snow albedo shows that the value over snow and ice is not necessarily 0.6 as assumed for the original TROPOMI product. For many areas in North America this can be as high as 0.9, however, over the boreal forest the reflectance is relatively low (0.2-0.3) even with snow cover.

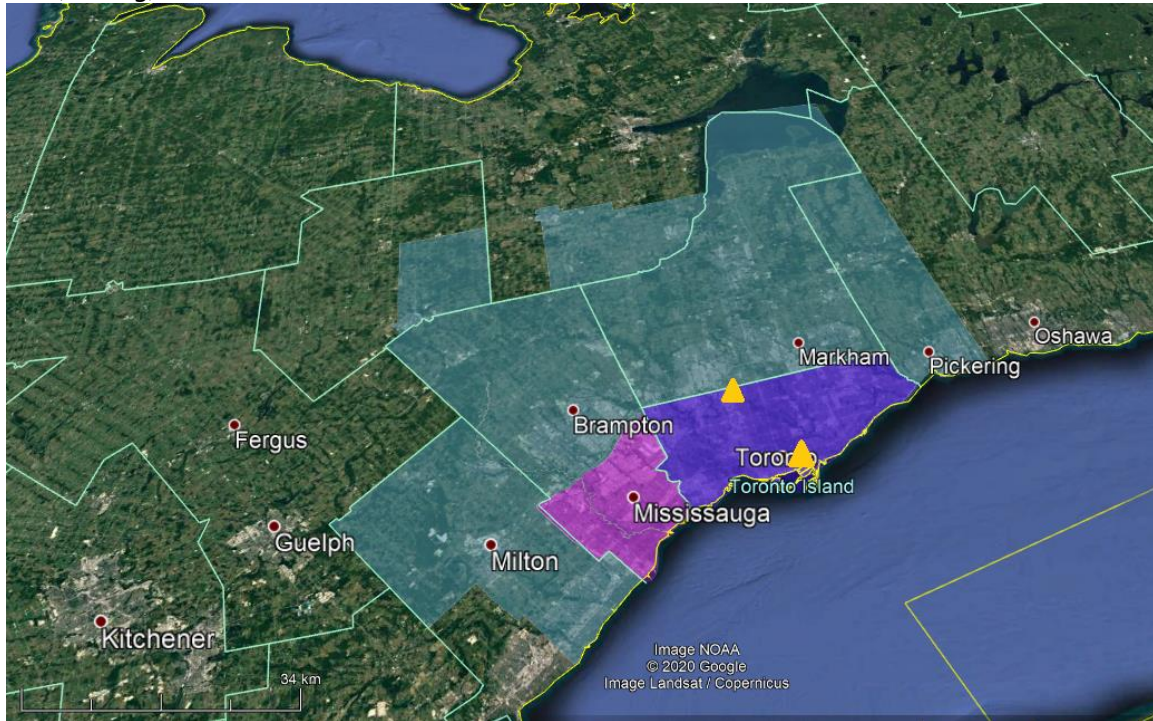


Figure S1. Boundaries of the Greater Toronto Area (GTA), shaded in grey. The Toronto and Mississauga city boundaries (used for the time series) are highlighted in violet and magenta, respectively. The orange triangles indicate the location of the ground-based PANDORA instruments (used for the evaluation of the satellite and model VCDs in Figs. S 8 and 9).

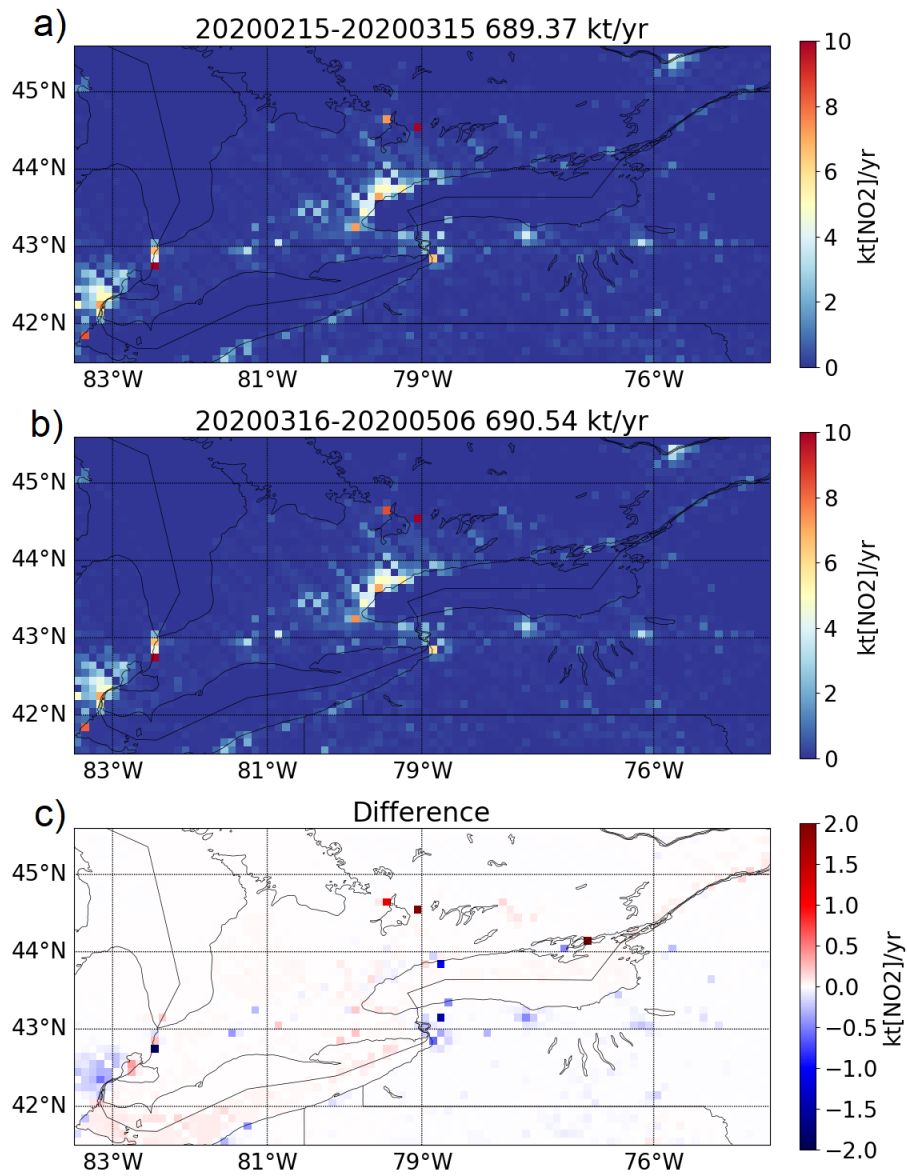


Figure S2. The figures show the operational forecast model's seasonal emission changes from the pre-lockdown (a) versus lockdown (b) period, the difference is shown in panel (c). Over the whole domain there is little change, however, in some area emissions decrease and in other increase slightly. The emissions shown here are the averaged emissions between 18-21 UTC.

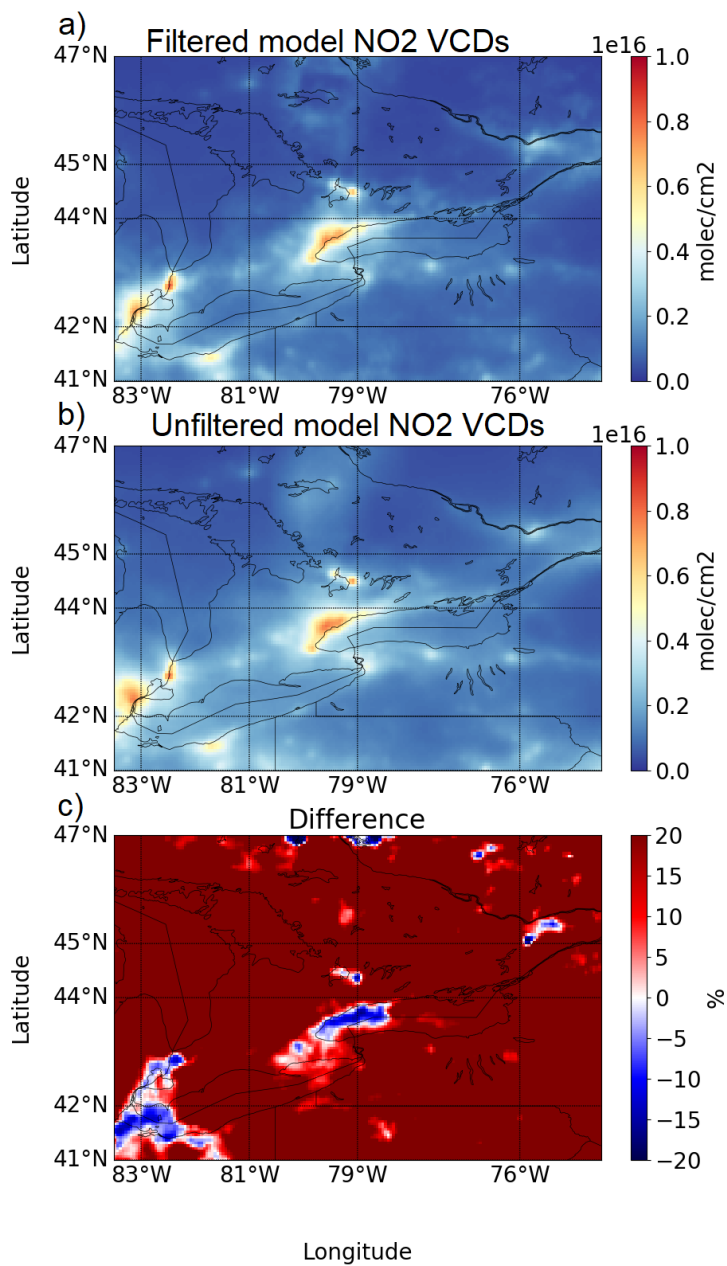


Figure S3. Impact of the sampling on the averaged TROPOMI columns. Model VCDs (a) filtered (like TROPOMI with $q_a > 0.75$) and (b) unfiltered (still sampled like TROPOMI) NO₂ VCDs over southern Ontario averaged over the lockdown time period, 16 March - May 6 for 2020. Panel (c) shows the difference (in %) between panels (a) and (b).

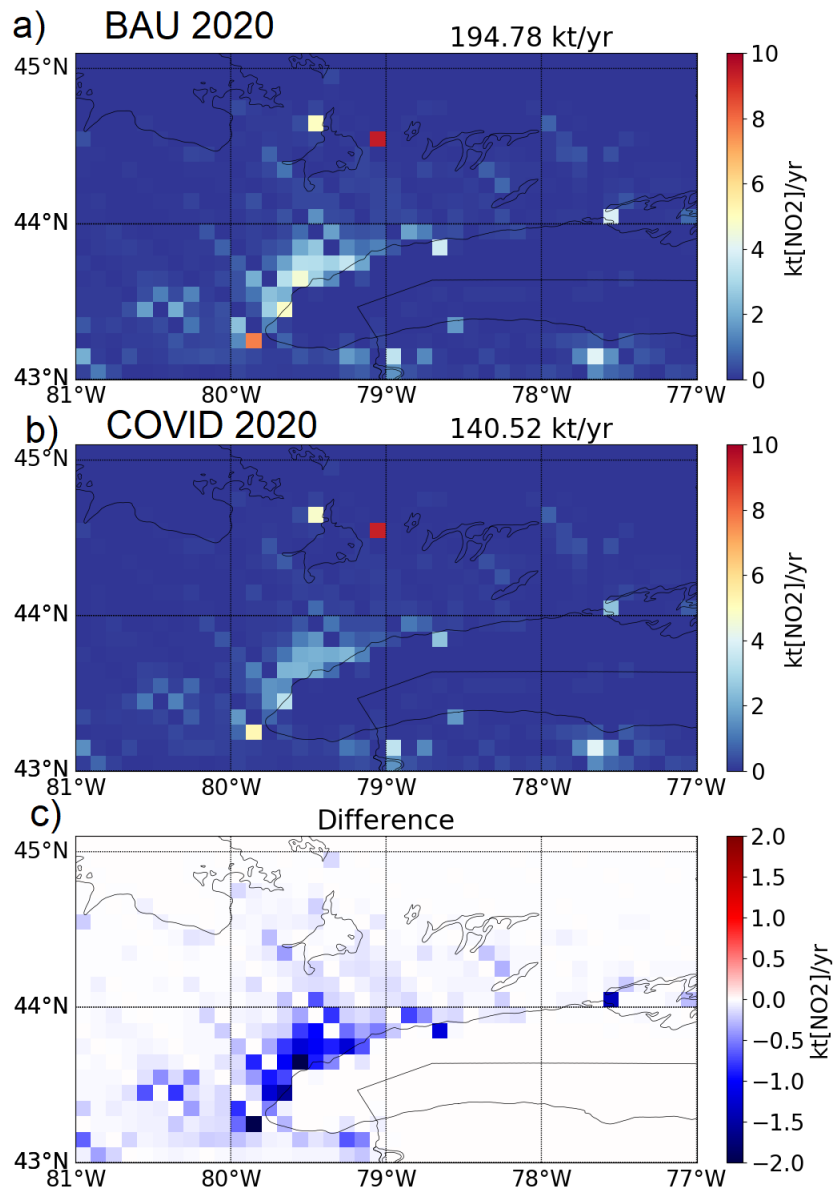


Figure S4. The model input NO_x emissions, binned to 0.1°x0.1°, in southern Ontario for (a) the 2020 business-as-usual emissions scenario and (b) the 2020 lockdown emissions scenario, assuming: (i) a 30% reduction in industry, (ii) a 60% reduction for traffic, (iii) 80% reduction in aircraft, and (iv) 20% increase of residential fuel combustion. The difference between BAU and the COVID scenario emissions is shown in panel (c). The emissions shown here are the averaged emissions between 18-21 UTC.

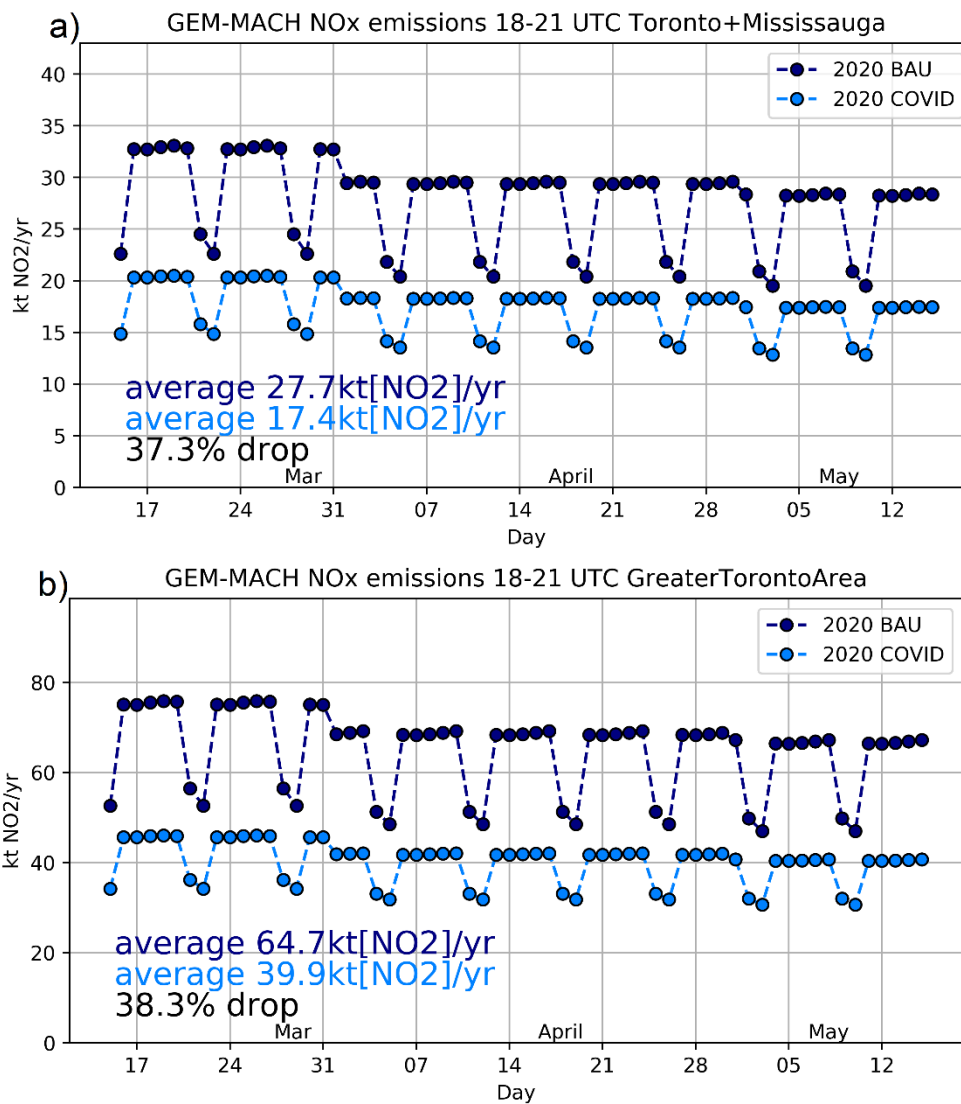


Figure S5. The model input NO_x emissions summed over the Toronto and Mississauga city (a) and GTA (b) boundaries, for the 2020 business-as-usual emissions scenario (navy) and the 2020 lockdown emissions scenario (blue), assuming: (i) a 30% reduction in industry, (ii) a 60% reduction for traffic, (iii) 80% reduction in aircraft, and (iv) 20% increase of residential fuel combustion. The emissions shown here are the averaged emissions between 18-21 UTC. Input emissions differ by day of week and by month.

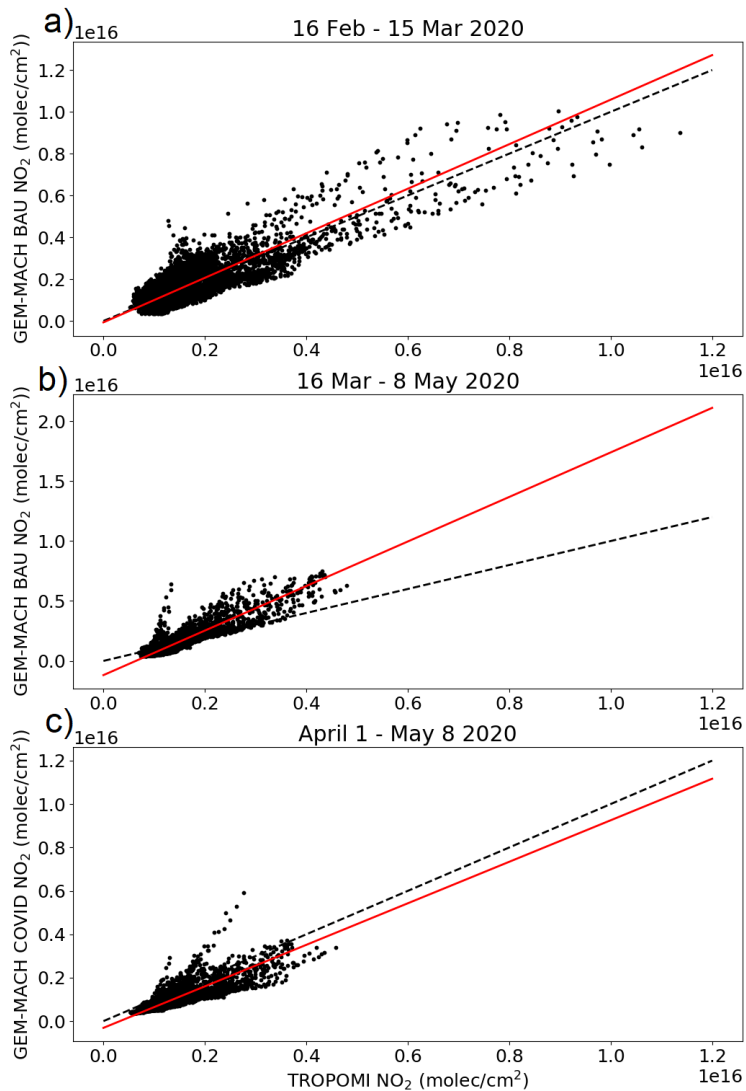


Figure S6. The correlation between the TROPOMI observations and the model NO₂ VCDs is shown in this figure (the statistics results can be found in Table S₃). The line of best fit is shown as a red line and the 1-to-1 line is shown as a back-dashed line (as a reference). Panel (a) shows the pre-lockdown period (16 February – 15 March 2020), and panel (b) the lock-down period (16 March – 8 May 2020) over southern Ontario using the 2020 BAU emissions (using the same dataset as shown in Fig. 1). There is good agreement in the pre-lockdown period, but the modeled columns are almost twice as large for the lockdown period. Panel (c) shows the comparison between TROPOMI and the model with the COVID scenario emissions (1 April – 8 May 2020; same dataset as shown in Fig. 3). The line-of-best fit is very close to the 1-to-1 line.

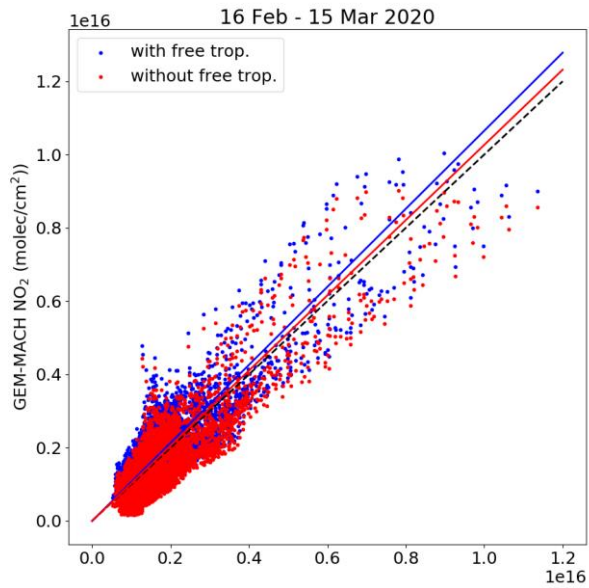


Figure S7. The correlation between the TROPOMI observations and the model NO₂ VCDs is shown in this figure pre-lockdown period (16 February – 15 March 2020, using the averages from Fig. 1 a and d). The blue dots are the model VCDs with the free troposphere added and the red dots are purely the GEM-MACH VCDs. The line of best fit is shown as a solid line and the 1-to-1 line is shown as a back-dashed line (as a reference). The free tropospheric VCDs are very small and don't impact the overall results much, however, assuming zero for the free troposphere is not correct.

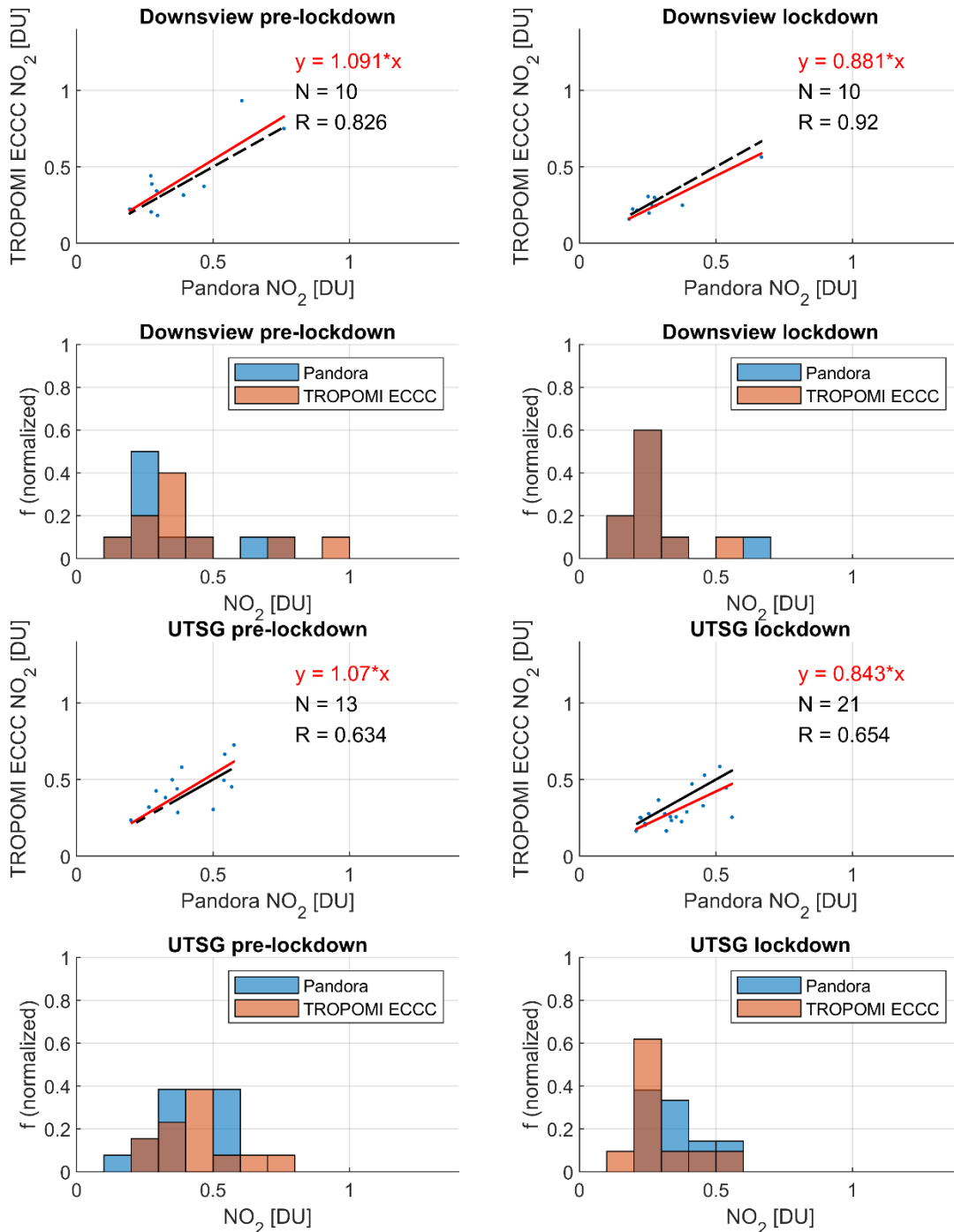


Figure S8. Comparison between TROPOMI NO₂ observations and ground-based PANDORA NO₂ measurements for the pre-lockdown and lockdown period in 2020, following the exact methodology as presented in Zhao et al., 2020 (simple coincident criteria). The location of the PANDORA sites is indicated in Fig. S1 as orange triangles (Downsview in north Toronto and UTGS in downtown Toronto). This shows overall good agreement between the ground-based and satellite-borne observations for the 2020 lockdown and pre-lockdown period.

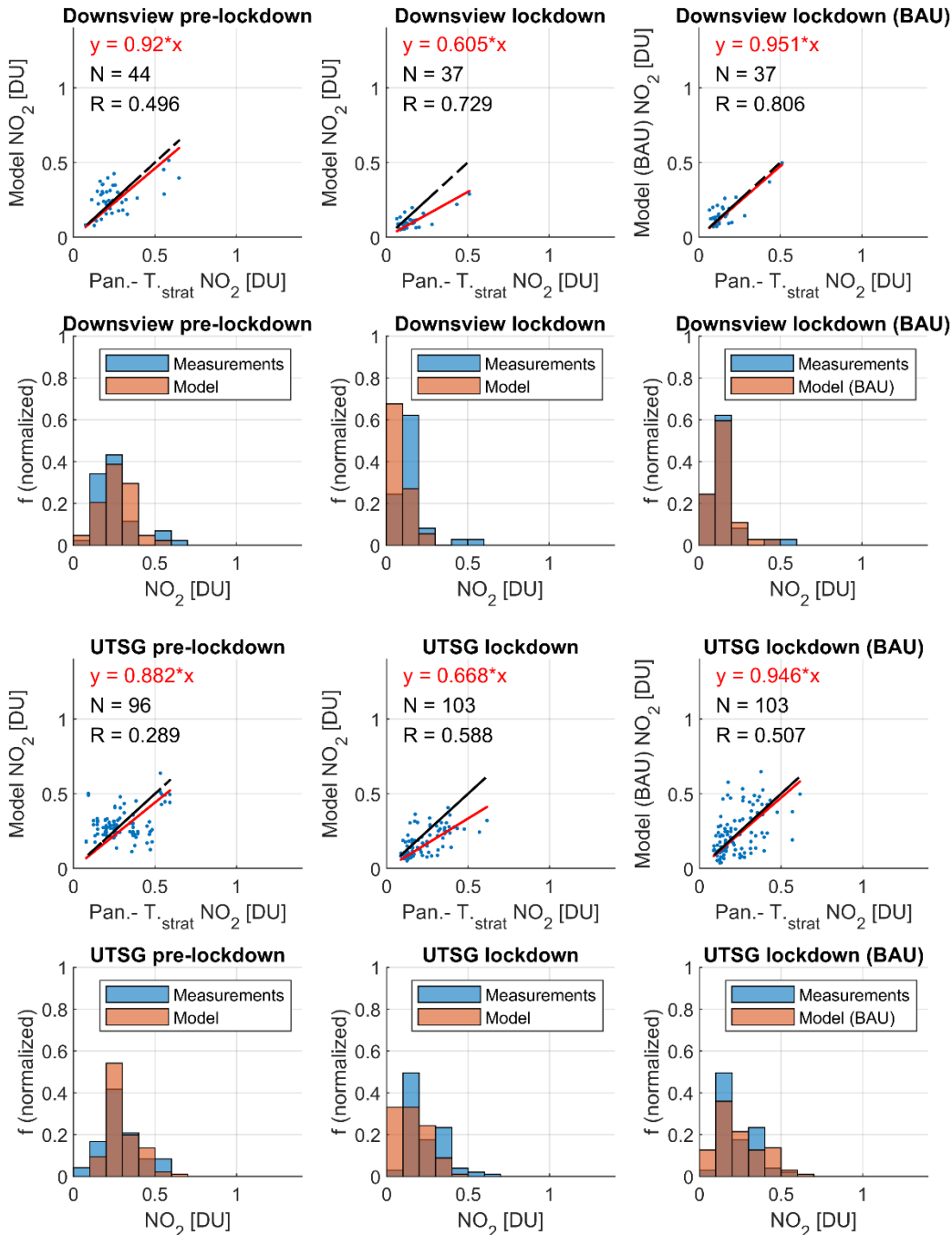


Figure S9. Comparison between model NO₂ VCDs and ground-based PANDORA NO₂ measurements for the pre-lockdown and lockdown period in 2020, following the exact methodology as presented in Zhao et al., 2020. To account for the missing stratospheric part in the model, the PANDORA total column NO₂ measurements were reduced by the daily TROPOMI stratospheric NO₂ (near the measurement site). Only model measurements near local noon (11 to 14 LST) were used for this evaluation to be consistent with the dataset used in this study. The location of the PANDORA sites is indicated in Fig. S1 as orange triangles (Downsview in north Toronto and UTGS in downtown Toronto). This shows overall good agreement between the ground-based observations and model output for the 2020 lockdown and pre-lockdown period.

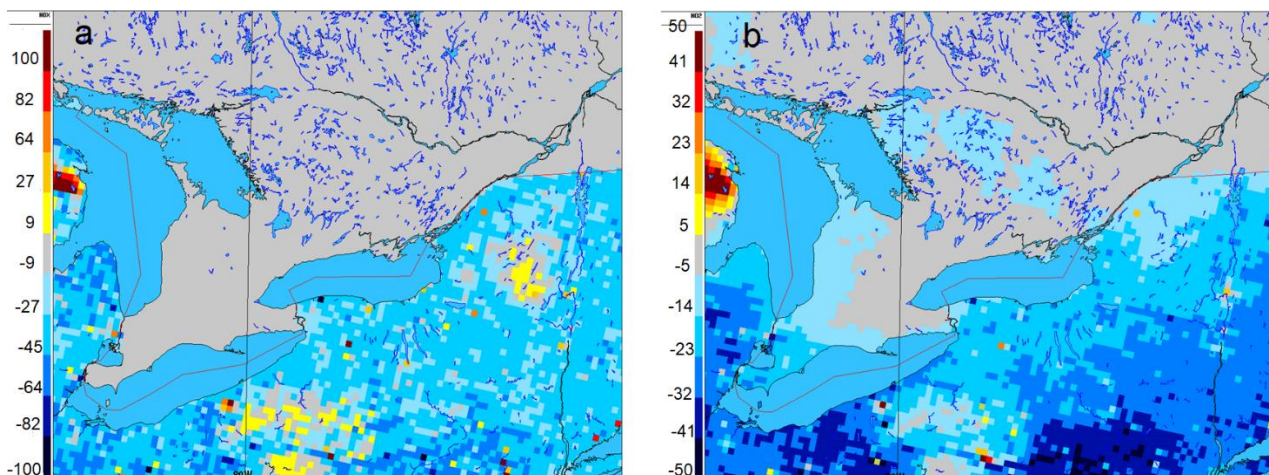


Figure S10. The impact of NO₂ emissions changes in the US on Canada is evaluated over the lockdown period (22 March 2020 to 10 May, 2020). The model input emissions are unchanged in Canada, but for the US emissions a 2017 and a projected 2028 scenario was compared. Panel (a) shows the % difference between the model input emissions (using 2017 US emissions versus 2028 projected US emissions, overall there is a decrease between 2017 to 2028, ranging between 27 to 45% (with the exception of a few locations; BAU 2028- BAU 2017). Panel (b) displays the % change in daily average NO₂ concentration averaged over the COVID period (2020-03-21 to 2020-05-10), predicted by GEM-MACH model for BAU scenario using the USA 2028 emissions vs 2017 emissions. The impact on the GTA is less than 5%. This shows that the impact from the US NO_x emissions on the GTA is negligible, given the short atmospheric lifetime of NO_x.

Table S2. Approximate average emissions (in t/d) used for the model run separated by sector during the lockdown period summed over the GTA.

Scenario	Species	Industry (-30%)	Road Transport (-60%)	Air Traffic (-80%)	Residential Heating (+20%)	Others (no change)	Total
BAU	NO _x	41	70	5	16	60	192
COVID	NO _x	29	28	1	19	60	137
BAU	VOC	75	18	1	4	136	234
COVID	VOC	52	7	0.2	4.3	136	200
BAU	PM _{2.5}	56	34	0.1	5	8	103
COVID	PM _{2.5}	39	14	0	6	8	67

Table S3. The statistics from Figure S6 (using a geometric mean). The difference is calculated as model- TROPOMI VCDs.

Panel (Fig.S6)	Slope	intersect	R	Difference	Std	RMSE
a	1.07	-6.77E+13	0.85	6.30E+13	6.94E+14	6.97E+14
b	1.86	-1.18E+15	0.90	8.46E+13	6.54E+14	6.59E+14
c	0.96	-3.10E+14	0.83	-3.72E+14	3.49E+14	5.10E+14

References

Bey, I., Jacob, D. J., Yantosca, R. M., Logan, J. A., Field, B. D., Fiore, A. M., et al. (2001). Global modeling of tropospheric chemistry with assimilated meteorology: Model description and evaluation. *Journal of Geophysical Research*, 106(D19), 23,073–23,095. <https://doi.org/10.1029/2001JD000807>

[Boersma, K. F., Eskes, H. J., Veefkind, J. P., Brinksma, E. J., van der A, R. J., Sneep, M., van den Oord, G. H. J., Levelt, P. F., Stammes, P., Gleason, J. F., and Bucsela, E. J. \(2007\), Near-real time retrieval of tropospheric NO₂ from OMI, *Atmos. Chem. Phys.*, 7, 2103–2118, <https://doi.org/10.5194/acp-7-2103-2007>.](https://doi.org/10.5194/acp-7-2103-2007)

[Bourassa, A., Degenstein, D., & Llewellyn, E. \(2008\). SASKTRAN: A spherical geometry radiative transfer code for efficient estimation of limb scattered sunlight. *Journal of Quantitative Spectroscopy and Radiative Transfer*, 109\(1\), 52–73. <https://doi.org/10.1016/j.jqsrt.2007.07.007>](https://doi.org/10.1016/j.jqsrt.2007.07.007)

Coats, C. J. (1996). High-performance algorithms in the Sparse Matrix Operator Kernel Emissions (SMOKE) Modeling System, American Meteorological Society, Atlanta, GA. USA, proceedings of the Ninth AMS Joint Conference on Applications of Air Pollution Meteorology with AWMA, 28 January–2 February 1996.

Cooper, M. J., R. V. Martin, A. I. Lyapustin, and C. A. McLinden (2018), Assessing snow extent data sets over North America to inform and improve trace gas retrievals from solar backscatter, *Atmospheric Measurement Techniques*, 11(5), 2983–2994, doi: 10.5194/amt-11-2983-2018.

Côté, J., Gravel, S., Méthot, A., Patoine, A., Roch, M., & Staniforth, A. (1998). The Operational CMC-MRB Global Environmental Multiscale (GEM) Model. Part I: Design Considerations and Formulation. *Monthly Weather Review*, 126(6), 1373–1395. [https://doi.org/10.1175/1520-0493\(1998\)126<1373:TOCMGE>2.0.CO;2](https://doi.org/10.1175/1520-0493(1998)126<1373:TOCMGE>2.0.CO;2)

- Dueck, S. R., Bourassa, A. E., & Degenstein, D. A. (2017). An efficient algorithm for polarization in the SASKTRAN radiative transfer framework. *Journal of Quantitative Spectroscopy and Radiative Transfer*, 199, 1–11. <https://doi.org/10.1016/j.jqsrt.2017.05.016>
- Girard, C., Plante, A., Desgagné, M., McTaggart-Cowan, R., Côté, J., Charron, M., et al. (2014). Staggered vertical discretization of the Canadian Environmental Multiscale (GEM) Model using a coordinate of the log-hydrostatic-pressure type. *Monthly Weather Review*, 142(3), 1183–1196. <https://doi.org/10.1175/MWR-D-13-00255.1>
- Gong, W.; Makar, P.; Zhang, J.; Milbrandt, J.; Gravel, S.; Hayden, K.; Macdonald, A.; Leitch, W. (2015). Modelling aerosol–cloud–meteorology interaction: A case study with a fully coupled air quality model (GEM-MACH). *Atmospheric Environment*, 115, 695 – 715. doi:<https://doi.org/10.1016/j.atmosenv.2015.05.062>.
- Gong, W.; Beagley, S.R.; Cousineau, S.; Sassi, M.; Munoz-Alpizar, R.; Ménard, S.; Racine, J.; Zhang, J.; Chen, J.; Morrison, H.; Sharma, S.; Huang, L.; Bellavance, P.; Ly, J.; Izdebski, P.; Lyons, L.; Holt, R. (2018). Assessing the impact of shipping emissions on air pollution in the Canadian Arctic and northern regions: current and future modelled scenarios. *Atmospheric Chemistry and Physics*, 18, 16653–16687. doi:10.5194/acp-18-16653-2018.
- Griffin, D.; Zhao, X.; McLinden, C.A.; Boersma, F.; Bourassa, A.; Dammers, E.; Degenstein, D.; Eskes, H.; Fehr, L.; Fioletov, V.; Hayden, K.; Kharol, S.K.; Li, S.M.; Makar, P.; Martin, R.V.; Mihele, C.; Mittermeier, R.L.; Krotkov, N.; Sneep, M.; Lamsal, L.N.; Linden, M.t.; van Geffen, J.; Veefkind, P.; Wolde, M. (2019): High-Resolution Mapping of Nitrogen Dioxide With TROPOMI: First Results and Validation Over the Canadian Oil Sands. *Geophysical Research Letters*, 46, 1049-1060, doi:10.1029/2018GL081095.
- Helfrich, S. R., D. McNamara, B. H. Ramsay, T. Baldwin, and T. Kasheta (2007), Enhancements to, and forthcoming developments in the Interactive Multisensor Snow and Ice Mapping System (IMS), *Hydrological Processes*, 21(12), 1576–1586, doi: 10.1002/hyp.6720.
- Houyoux, M.R.; Vukovich, J.M.; Coats Jr., C.J.; Wheeler, N.J.M.; Kasibhatla, P.S. (2000). Emission inventory development and processing for the Seasonal Model for Regional Air Quality (SMRAQ) project. *Journal of Geophysical Research: Atmospheres*, 105, 9079–9090, [<https://agupubs.onlinelibrary.wiley.com/doi/pdf/10.1029/1999JD900975>]. doi:10.1029/1999JD900975.
- Makar, P., Gong, W., Hogrefe, C., Zhang, Y., Curci, G., Zabkar, R., et al. (2015b). Feedbacks between air pollution and weather, part 2: Effects on chemistry. *Atmospheric Environment*, 115, 499–526. <https://doi.org/10.1016/j.atmosenv.2014.10.021>
- Makar, P., Gong, w., Milbrandt, J., Hogrefe, C., Zhang, Y., Curci, G., et al. (2015a). Feedbacks between air pollution and weather, Part 1: Effects on weather. *Atmospheric Environment*, 115, 442–469.

Martin, R. V., K. Chance, D. J. Jacob, T. P. Kurosu, R. J. D. Spurr, E. Bucsel, J. F. Gleason, P. I. Palmer, I. Bey, A. M. Fiore, Q. Li, R. M. Yantosca, and R. B. A. Koelemeijer (2002), An improved retrieval of tropospheric nitrogen dioxide from GOME, *Journal of Geophysical Research: Atmospheres*, 107(D20), ACH 9–1–ACH 9–21, doi:10.1029/2001JD001027.

McLinden, C. A., Fioletov, V., Boersma, K. F., Kharol, S. K., Krotkov, N., Lamsal, L., et al. (2014). Improved satellite retrievals of NO₂ and SO₂ over the Canadian oil sands and comparisons with surface measurements. *Atmospheric Chemistry and Physics*, 14(7), 3637–3656.
<https://doi.org/10.5194/acp-14-3637-2014>

Moran, M.D.; Ménard, S. Regional Air Quality Deterministic Prediction System (RAQDPS): Update from version 020.2 to version 021; Canadian Centre for Meteorological and Environmental Prediction: Montreal, CA, 2019. Technical note, p. 49 pp.,
http://collaboration.cmc.ec.gc.ca/cmc/cmoe/product_guide/docs/tech_notes/technote_raqdps-021_20190703_e.pdf [last access: 23 June 2020].

Moran, M. D., Ménard, S., Talbot, D., Huang, P., Makar, P. A., Gong, W., et al. (2010). Particulate-matter forecasting with GEM-MACH15, A New Canadian Air-quality Forecast Model, in: *Air pollution modelling and its application XX*. Dordrecht, the Netherlands: Springer.

Palmer, P. I., D. J. Jacob, K. Chance, R. V. Martin, R. J. D. Spurr, T. P. Kurosu, I. Bey, R. Yantosca, A. Fiore, and Q. Li (2001), Air mass factor formulation for spectroscopic measurements from satellites: Application to formaldehyde retrievals from the Global Ozone Monitoring Experiment, *Journal of Geophysical Research: Atmospheres*, 106(D13), 14,539–14,550, doi:10.1029/2000JD900772.

Pavlovic, R.; Chen, J.; Anderson, K.; Moran, M.D.; Beaulieu, P.A.; Davignon, D.; Cousineau, S. (2016). The FireWork air quality forecast system with near-real-time biomass burning emissions: Recent developments and evaluation of performance for the 2015 North American wildfire season. *Journal of the Air & Waste Management Association*, 66, 819–841, [https://doi.org/10.1080/10962247.2016.1158214]. PMID: 337 26934496, doi:10.1080/10962247.2016.1158214.

Pendlebury, D., Gravel, S., Moran, M. D., & Lupu, A. (2018). Impact of chemical lateral boundary conditions in a regional air quality forecast model on surface ozone predictions during stratospheric intrusions. *Atmospheric Environment*, 174, 148–170.
<https://doi.org/10.1016/j.atmosenv.2017.10.052>.

Schaaf, C. B., Gao, F., Strahler, A. H., Lucht, W., Li, X., Tsang, T., et al. (2002). First operational BRDF, albedo nadir reflectance products from MODIS. *Remote Sensing of Environment*, 83(1), 135–148. [https://doi.org/10.1016/S0034-4257\(02\)00091-3](https://doi.org/10.1016/S0034-4257(02)00091-3), the Moderate Resolution Imaging Spectroradiometer (MODIS): A new generation of Land Surface Monitoring.

Zhang, J., Moran, M. D., Zheng, Q., Makar, P. A., Baratzadeh, P., Marson, G., et al. (2018). Emissions preparation and analysis for multiscale air quality modeling over the Athabasca Oil Sands Region of Alberta, Canada. *Atmospheric Chemistry and Physics*, 18(14), 10,459–10,481. <https://doi.org/10.5194/acp-18-10459-2018>

Zawada, D. J., Dueck, S. R., Rieger, L. A., Bourassa, A. E., Lloyd, N. D., & Degenstein, D. A. (2015). High-resolution and monte carlo additions to the Sasktran radiative transfer model. *Atmospheric Measurement Techniques*, 8(6), 2609–2623. <https://doi.org/10.5194/amt-8-2609-2015>